Available online at www.sciencedirect.com
ScienceDirect
Journal of Solid State Chemistry 180 (2007) 2581–2586
JOURNAL OF SOLID STATE CHEMISTRY
www.elsevier.com/locate/jssc

Syntheses, structure, magnetism, and optical properties of the partially ordered quaternary interlanthanide sulfides $PrLnYb_2S_6$ (Ln = Tb, Dy)

Geng Bang Jin[a], Eun Sang Choi[b], Robert P. Guertin[c], James S. Brooks[b], Corwin H. Booth[d], Thomas E. Albrecht-Schmitt[a,*]

[a]Department of Chemistry and Biochemistry and the E.C. Leach Nuclear Science Center, Auburn University, Auburn, AL 36849, USA
[b]Department of Physics and National High Magnetic Field Laboratory, Florida State University, Tallahassee, FL 32310, USA
[c]Department of Physics and Astronomy, Tufts University, Medford, MA 02155, USA
[d]Chemical Sciences Division, Lawrence Berkeley National Laboratory, 1 Cyclotron Road, Berkeley, CA 94720, USA

Received 7 May 2007; received in revised form 6 June 2007; accepted 10 June 2007
Available online 21 July 2007

Abstract

Dark red single crystals of $PrLnYb_2S_6$ (Ln = Pr/Yb, Tb, Dy) have been synthesized through the reactions of elemental rare earth metals and S using a Sb_2S_3 flux at 1000 °C. These isotypic compounds adopt the F-Ln_2S_3 three-dimensional open-channel structure type. Eight-coordinate Pr^{3+} ions sit in the channels that are constructed from three different edge-shared double chains running down the b-axis that contain $Yb(1)S_6$ octahedra, $Yb(2)S_6$ octahedra, and LnS_7 monocapped trigonal prisms. Each double chain connects to four other neighbors by sharing vertices and edges. Considerable disordering in Ln positions was observed in single X-ray diffraction experiments only in the case of Pr/Yb. Least-squares refinements gave rise to the formulas of $Pr_{1.34}Yb_{2.66}S_6$, of $PrTbYb_2S_6$, and $PrDyYb_2S_6$, which are confirmed by the elemental analysis and magnetic susceptibility measurements. $Pr_{1.34}Yb_{2.66}S_6$, $PrTbYb_2S_6$, and $PrDyYb_2S_6$ are paramagnetic down to 2 K, without any indications of long-range magnetic ordering. The optical transitions for $Pr_{1.34}Yb_{2.66}S_6$, $PrTbYb_2S_6$, and $PrDyYb_2S_6$ are at approximately 1.6 eV. Crystallographic data are listed as an example for $PrTbYb_2S_6$: monoclinic, space group $P2_1/m$, $a = 10.9496(10)$ Å, $b = 3.9429(4)$ Å, $c = 11.2206(10)$ Å, $\beta = 108.525(2)°$, $V = 459.33(7)$ Å^3, $Z = 2$.

Keywords: Interlanthanide sulfide; Mixed-lanthanide sulfide

1. Introduction

There have been numerous studies on ternary interlanthanide chalcogenides in terms of their diverse structural chemistry and interesting physical properties [1–18]. α-$LnLn'S_3$ [1–4] ($GdFeO_3$ type [19]), $CeYb_3S_6$ [5,6] (F-Ln_2S_3 type [20,21]), $Sc_2Er_3S_7$ [7] (Y_5S_7 type [22]) and $EuLn_2Q_4$ [8–10] ($CaFe_2O_4$ type [23]) possess three-dimensional open-channel structures, wherein the larger Ln^{3+} ions reside in channels formed by smaller lanthanide chalcogenide polyhedra. While β-$LnLn'Q_3$ (Q = S, Se) [3,11,12] ($UFeS_3$ type [24]), and γ-$LnLn'S_3$ (Ln = La, Ce; Ln' = Er, Tm, Yb) [13] have layers of $Ln'Q_x$ polyhedra, separated by larger Ln^{3+} ions. δ-$LnLuS_3$ (Ln = Ce, Pr, Nd) [14] ($CeTmS_3$ type [15]) have a very condensed three-dimensional structure. Recent work has shown that the electronic and magnetic properties of these materials depend highly on the structures they adopt and the choices of lanthanides. For example, the optical band gap of γ-$LnLn'S_3$ (Ln = La, Ce; Ln' = Er, Tm, Yb) [13] are approximately 1.3–1.6 eV, while $SmEr_3S_6$ is 2.4–2.6 eV [16]. δ-$LnLuS_3$ (Ln = Pr, Nd) exhibit possible short-range antiferromagnetic ordering at low temperatures [14].

In contrast, there are no existing ordered quaternary interlanthanide chalcogenides that possess three different lanthanide elements. Instead of searching for new ordered quaternary phases, there are known ternary interlanthanide sulfide structure types that might accommodate three different lanthanide ions in an ordered arrangement. F-Ln_2S_3-type [17,18] ternary compounds are probably the best candidates to achieve this goal. This structure type has

*Corresponding author.
E-mail address: albreth@auburn.edu (T.E. Albrecht-Schmitt).

0022-4596/$ - see front matter © 2007 Elsevier Inc. All rights reserved.
doi:10.1016/j.jssc.2007.06.032

three different coordination environments for Ln^{3+} as octahedral, and mono- and bicapped trigonal prisms. The metal atoms are often disordered on seven-coordinate sites. By carefully choosing three different metals, ordered quaternary phases might be accessible. In this paper, we present the syntheses, structure, optical and magnetic properties of the first two partially ordered quaternary interlanthanide chalcogenides, $PrTbYb_2S_6$ and $PrDyYb_2S_6$. As a reference, $Pr_{1.34}Yb_{2.66}S_6$ is also included in the discussion.

2. Experimental section

2.1. Starting materials

Pr (99.9%, Alfa-Aesar), Tb (99.9%, Alfa-Aesar), Dy (99.9%, Alfa-Aesar), Yb (99.9%, Alfa-Aesar), S (99.5%, Alfa-Aesar), and Sb (99.5%, Alfa-Aesar) were used as received. The Sb_2S_3 flux was prepared from the direct reaction of the elements in sealed fused-silica ampoules at 850 °C.

2.2. Syntheses

Pr*Ln*Yb_2S_6 (*Ln* = Tb, Dy) were prepared through the reaction of Pr (0.17 mmol), *Ln* (0.17 mmol), Yb (0.34 mmol), S (1.02 mmol), and Sb_2S_3 (0.17 mmol). For $Pr_{1.34}Yb_{2.66}S_6$, the reaction mixture consists of Pr (0.23 mmol), Yb (0.45 mmol), S (1.02 mmol), and Sb_2S_3 (0.17 mmol). All of the reactants were loaded into fused-silica ampoules under an argon atmosphere in a glovebox. The ampoules were sealed under vacuum and heated in a programmable tube furnace. The following heating profile was used: 2 °C/min to 500 °C (held for 1 h), 0.5 °C/min to 1000 °C (held for 5 d), 0.04 °C/min to 550 °C (held for 2 d), and 0.5 °C/min to 24 °C. Powder X-ray diffraction measurements were used to confirm phase purity by comparing the powder patterns calculated from the single-crystal X-ray structures with the experimental diffraction data. Semi-quantitative SEM/EDX analyses were performed using a JEOL 840/Link Isis or JEOL JSM-7000F instrument. Pr, *Ln*, Yb, and S percentages were calibrated against standards. Sb was not detected in the crystals. Pr:*Ln*:Yb:S ratios of close to 1:1:2:6 were found for Pr*Ln*Yb_2S_6 (*Ln* = Tb, Dy), while the Pr:Yb:S ratios in $Pr_{1.34}Yb_{2.66}S_6$ samples are approximately 1:2:4.5 from EDX analyses.

2.3. Crystallographic studies

Single crystals of Pr*Ln*Yb_2S_6 (*Ln* = Pr/Yb, Tb, Dy) were mounted on glass fibers with epoxy and optically aligned on a Bruker APEX single-crystal X-ray diffractometer using a digital camera. Initial intensity measurements were performed using graphite monochromated Mo *Kα* ($\lambda = 0.71073$ Å) radiation from a sealed tube and monocapillary collimator. SMART (v 5.624) was used for preliminary determination of the cell constants and data collection control. The intensities of reflections of a sphere were collected by a combination of 3 sets of exposures (frames). Each set had a different ϕ angle for the crystal and each exposure covered a range of 0.3° in ω. A total of 1800 frames were collected with exposure times per frame of 10 or 20 s depending on the crystal.

For Pr*Ln*Yb_2S_6 (*Ln* = Pr/Yb, Tb, Dy), determination of integrated intensities and global refinement were performed with the Bruker SAINT (v 6.02) software package using a narrow-frame integration algorithm. These data were treated first with a face-indexed numerical absorption correction using XPREP [25], followed by a semi-empirical absorption correction using SADABS [26]. The program suite SHELXTL (v 6.12) was used for space group determination (XPREP), direct methods structure solution (XS), and least-squares refinement (XL) [25]. The final refinements included anisotropic displacement parameters for all atoms and secondary extinction. Some crystallographic details are given in Table 1. Atomic coordinates, occupancies, and equivalent isotropic displacement parameters for Pr*Ln*Yb_2S_6 (*Ln* = Pr/Yb, Tb, Dy) are given in Tables 2–4. Additional crystallographic details can be found in the Supporting Information.

The formula of F-Ln_2S_3-type compounds can be expressed as $(A^{VIII})(B^{VII})(C^{VI})_2S_6$, where the superscripts represent the coordination numbers of each site. In the case of $Pr_{1.34}Yb_{2.66}S_6$, eight-coordinate *A* sites were assigned as Pr atoms and both of seven-coordinate *B* and octahedral *C* positions were named as Yb at the beginning of the refinement. However the average bond distance of YbS_7 is longer than the tabulated value, according to Shannon's radii data [27], and its thermal parameter is larger than the other Yb atoms. The elementary analysis showed that the ratio of Pr:Yb is 1:2. These data suggest that there should

Table 1
Crystallographic data for Pr*Ln*Yb_2S_6 (*Ln* = Pr/Yb, Tb, Dy)

Formula	$Pr_{1.34}Yb_{2.66}S_6$	$PrTbYb_2S_6$	$PrDyYb_2S_6$
Formula weight	841.31	838.27	841.85
Color	Dark red	Dark red	Dark red
Crystal system	Monoclinic	Monoclinic	Monoclinic
Space group	$P2_1/m$ (No. 11)	$P2_1/m$ (No. 11)	$P2_1/m$ (No. 11)
a (Å)	10.960(2)	10.950(1)	10.938(1)
b (Å)	3.9501(8)	3.9429(4)	3.9398(4)
c (Å)	11.220(2)	11.221(1)	11.204(1)
β (°)	108.545(3)	108.525(2)	108.612(2)
V (Å^3)	460.5(2)	459.33(7)	457.57(7)
Z	2	2	2
T (K)	193	193	193
λ (Å)	0.71073	0.71073	0.71073
ρ_{calcd} (g cm^{-3})	6.067	6.061	6.110
μ (cm^{-1})	349.71	342.64	348.32
Indep. reflections	1316	1282	1301
Parameters refined	63	62	62
$R(F)$[a]	0.0233	0.0330	0.0243
$R_w(F_o^2)$[b]	0.0657	0.1104	0.0597

[a] $R(F) = \sum||F_o| - |F_c||/\sum|F_o|$ for $F_o^2 > 2\sigma(F_o^2)$.
[b] $R_w(F_o^2) = [\sum[w(F_o^2 - F_c^2)^2]/\sum wF_o^4]^{1/2}$.

Table 2
Atomic coordinates and equivalent isotropic displacement parameters for $Pr_{1.34}Yb_{2.66}S_6$

Atom (site)	x	y	z	Occupancy	U_{eq} (Å^2)[a]
Pr1	0.55123(4)	1/4	0.19606(4)	1	0.0084(1)
Pr/Yb	0.18137(4)	1/4	0.00138(4)	0.34(1)/0.66(1)	0.0109(2)
Yb1	0.94227(3)	1/4	0.33496(3)	1	0.0100(1)
Yb2	0.65971(3)	1/4	0.58575(3)	1	0.0101(1)
S1	0.4186(2)	1/4	0.5937(2)	1	0.0086(4)
S2	0.8937(2)	1/4	0.5587(2)	1	0.0100(4)
S3	0.2334(2)	1/4	0.7695(2)	1	0.0090(4)
S4	0.3064(2)	1/4	0.2544(2)	1	0.0098(4)
S5	0.9805(2)	1/4	0.1160(2)	1	0.0121(4)
S6	0.6166(2)	1/4	0.9623(2)	1	0.0084(4)

[a] U_{eq} is defined as one-third of the trace of the orthogonalized U_{ij} tensor.

Table 3
Atomic coordinates and equivalent isotropic displacement parameters for $PrTbYb_2S_6$

Atom (site)	x	y	z	Occupancy	U_{eq} (Å^2)[a]
Pr1	0.55027(7)	1/4	0.19511(7)	1	0.0064(2)
Tb1	0.18125(6)	1/4	0.00196(6)	1	0.0075(2)
Yb1	0.94104(5)	1/4	0.33390(5)	1	0.0098(2)
Yb2	0.65988(5)	1/4	0.58556(5)	1	0.0096(2)
S1	0.4185(3)	1/4	0.5947(3)	1	0.0073(6)
S2	0.8943(3)	1/4	0.5591(3)	1	0.0085(6)
S3	0.2357(3)	1/4	0.7711(3)	1	0.0071(6)
S4	0.3064(3)	1/4	0.2532(3)	1	0.0095(6)
S5	0.9800(3)	1/4	0.1144(3)	1	0.0101(7)
S6	0.6159(3)	1/4	0.9625(3)	1	0.0081(6)

[a] U_{eq} is defined as one-third of the trace of the orthogonalized U_{ij} tensor.

Table 4
Atomic coordinates and equivalent isotropic displacement parameters for $PrDyYb_2S_6$

Atom (site)	x	y	z	Occupancy	U_{eq} (Å^2)[a]
Pr1	0.54996(5)	1/4	0.19506(5)	1	0.0080(1)
Dy1	0.18100(4)	1/4	0.00156(4)	1	0.0085(1)
Yb1	0.94108(4)	1/4	0.33369(4)	1	0.0105(1)
Yb2	0.66021(4)	1/4	0.58597(4)	1	0.0104(1)
S1	0.4181(2)	1/4	0.5945(2)	1	0.0087(5)
S2	0.8943(2)	1/4	0.5590(2)	1	0.0098(5)
S3	0.2348(2)	1/4	0.7715(2)	1	0.0088(4)
S4	0.3051(2)	1/4	0.2525(2)	1	0.0100(5)
S5	0.9799(2)	1/4	0.1140(2)	1	0.0101(5)
S6	0.6165(2)	1/4	0.9628(2)	1	0.0095(5)

[a] U_{eq} is defined as one-third of the trace of the orthogonalized U_{ij} tensor.

be a certain amount of disorder at the *B* site. Refinement of Pr/Yb occupancy at the *B* site lowered the residuals and weighting scheme, and gave rise to the final formula of $Pr_{1.34(1)}Yb_{2.66(1)}S_6$.

For $PrLnYb_2S_6$ (Ln = Tb, Dy), Pr, *Ln*, and Yb atoms were put in *A*, *B*, and *C* positions, respectively. This gave excellent residuals in the refinements and the suggested formulas as $PrLnYb_2S_6$ (Ln = Tb, Dy) are consistent with the EDX results. Considering the similar X-ray scattering factors of Pr, *Ln*, and Yb, disorder of these atoms cannot be excluded.

2.4. Powder X-ray diffraction

Powder X-ray diffraction patterns were collected with a Rigaku Miniflex powder X-ray diffractometer using Cu Kα ($\lambda = 1.54056$ Å) radiation.

2.5. Magnetic susceptibility measurements

Magnetism data were measured on powders in gelcap sample holders with a Quantum Design MPMS 7 T magnetometer/susceptometer between 2 and 300 K and in applied fields up to 7 T. DC susceptibility measurements were made under zero-field-cooled conditions with an applied field of 0.1 T. Susceptibility values were corrected for the sample diamagnetic contribution according to Pascal's constants [28] as well as for the sample holder diamagnetism. θ_p values were obtained from extrapolations from fits between 100 and 300 K.

2.6. UV–vis–NIR diffuse reflectance spectroscopy

The diffuse reflectance spectra of $PrLnYb_2S_6$ (Ln = Pr/Yb, Tb, Dy) were measured from 200 to 1500 nm using a Shimadzu UV3100 spectrophotometer equipped with an integrating sphere attachment. The Kubelka–Munk function was used to convert diffuse reflectance data to absorption spectra [29].

3. Results and discussion

3.1. Structures of $PrLnYb_2S_6$ (Ln = Pr/Yb, Tb, Dy)

The isotypic series of $PrLnYb_2S_6$ (Ln = Pr/Yb, Tb, Dy) have the F-Ln_2S_3-type structure with Pr^{3+} ions in eight-coordinate positions, Ln^{3+} ions in seven-coordinate positions, and Yb^{3+} ions occupying two different octahedral sites. The coordination geometries of these cations are shown in Fig. 1. The LnS_7 and PrS_8 polyhedra can be viewed as monocapped trigonal prisms and bicapped trigonal prisms, respectively. As shown in Fig. 2, the structure of these compounds is constructed from three different edge-shared double chains running down the *b*-axis that contain $Yb(1)S_6$ octahedra, $Yb(2)S_6$ octahedra, and LnS_7 monocapped trigonal prisms, respectively. Each double chain connects to four other neighbors by sharing vertices and edges to form the channels where the Pr^{3+} ions reside. For example, $Yb(1)S_6$ double chains are bound to two $Yb(2)S_6$ double chains via corner-sharing and two LnS_7 double chains via edge-sharing.

Selected interatomic distances for $PrLnYb_2S_6$ (Ln = Pr/Yb, Tb, Dy) are listed in Table 5. Pr–S bond distances range from 2.876(2) to 3.013(2) Å, which are comparable to

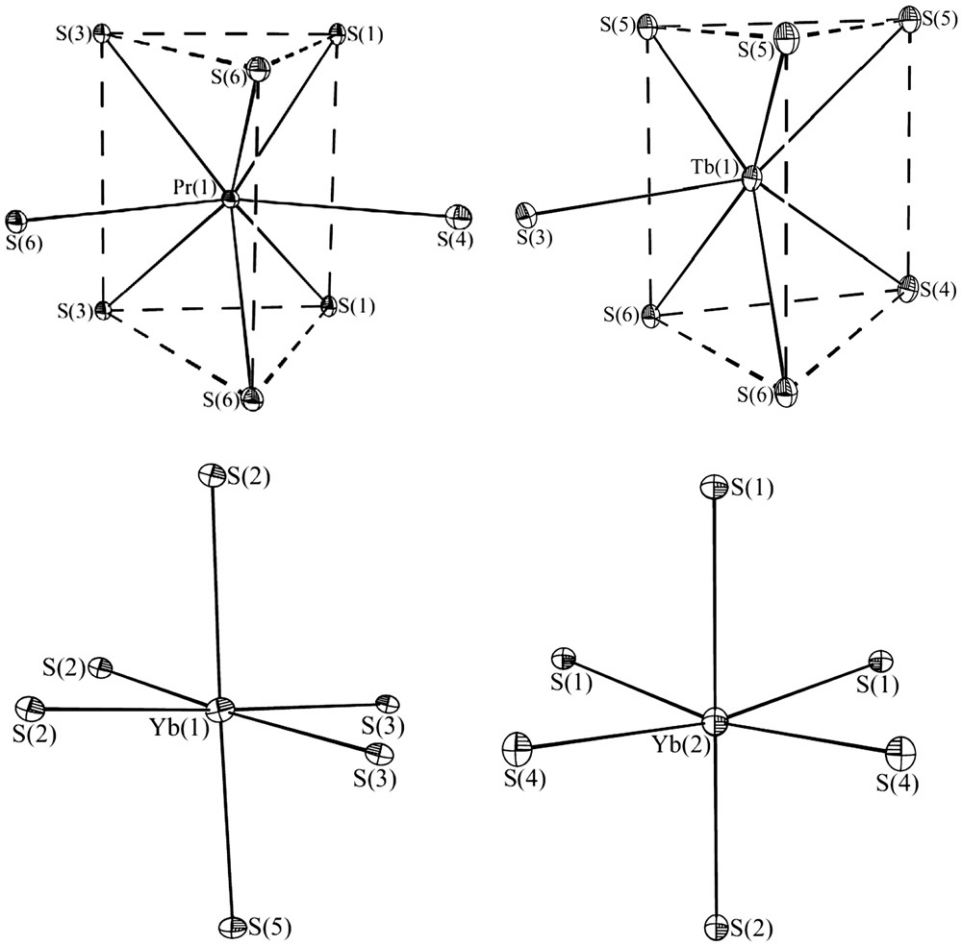

Fig. 1. A depiction of the coordination environments of the cations in $PrTbYb_2S_6$. 50% probability ellipsoids are shown.

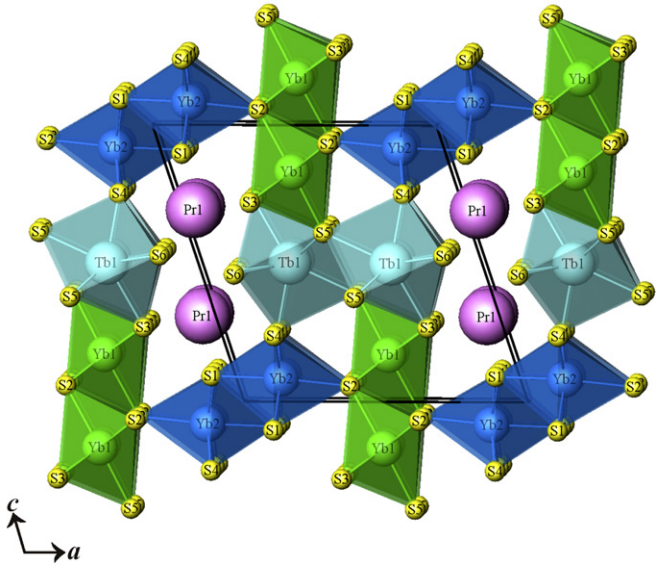

Fig. 2. An illustration of the three-dimensional structure of $PrTbYb_2S_6$ viewed along the *b*-axis.

Shannon's radii data of 2.966 Å [27]. The average bond distances for Pr/YbS_7, TbS_7, and DyS_7 are 2.807(2), 2.800(2), and 2.792(2) Å, respectively. Compared to the Shannon's radii values for PrS_7 (2.89 Å), YbS_7 (2.765 Å), TbS_7 (2.82 Å), and DyS_7 (2.81 Å), they are all reasonable [27]. The bond distances for YbS_6 octahedra are in the range of 2.613(1) and 2.759(2) Å.

3.2. Magnetic susceptibility

The magnetic susceptibilities for $PrLnYb_2S_6$ (Ln = Pr/Yb, Tb, Dy), in the range of 2–300 K, are presented in Figs. 3–5. There are no indications of long-range magnetic ordering down to 2 K. $Pr_{1.34}Yb_{2.66}S_6$ deviates from the ideal Curie–Weiss law below 70 K due to crystal-field splitting of lanthanide ions. $PrTbYb_2S_6$ shows pure Curie–Weiss paramagnetic behavior in the whole temperature range, while the $1/\chi$ plot for $PrDyYb_2S_6$ exhibits a deviation from the Curie–Weiss law, and the onset of upward curvature at low temperature. This may indicate short-range antiferromagnetic ordering that has also been observed in δ-$Pr_{1.29}Lu_{0.71}S_3$ [14]. Table 6 shows the magnetic parameters for $PrLnYb_2S_6$ (Ln = Pr/Yb, Tb, Dy) that were obtained from fitting the data in the range of 100–300 K into the Curie–Weiss law. All three compounds have negative values of θ_p, which indicates antiferromagnetic interactions between cations. The experimental

Table 5
Selected interatomic distances (Å) for Pr*Ln*Yb_2S_6 (*Ln* = Pr/Yb, Tb, Dy)

Formula	$Pr_{1.34}Yb_{2.66}S_6$	$PrTbYb_2S_6$	$PrDyYb_2S_6$
Pr(1)–S(1) × 2	3.013(2)	3.009(2)	3.006(2)
Pr(1)–S(3) × 2	3.007(2)	2.993(2)	3.000(2)
Pr(1)–S(4)	2.958(2)	2.943(3)	2.947(3)
Pr(1)–S(6) × 2	2.892(2)	2.877(2)	2.876(2)
Pr(1)–S(6)	2.930(2)	2.919(3)	2.918(2)
Ln–S(3)	2.836(2)	2.837(3)	2.821(2)
Ln–S(4)	2.732(2)	2.715(3)	2.704(3)
Ln–S(5) × 2	2.701(2)	2.692(2)	2.683(2)
Ln–S(5)	2.881(2)	2.865(3)	2.863(2)
Ln–S(6) × 2	2.898(2)	2.901(2)	2.895(2)
Yb(1)–S(2) × 2	2.682(2)	2.684(2)	2.681(2)
Yb(1)–S(2)	2.726(2)	2.734(3)	2.731(2)
Yb(1)–S(3) × 2	2.747(2)	2.752(2)	2.743(2)
Yb(1)–S(5)	2.620(2)	2.630(3)	2.628(2)
Yb(2)–S(1) × 2	2.756(2)	2.759(2)	2.756(2)
Yb(2)–S(1)	2.673(2)	2.678(3)	2.680(2)
Yb(2)–S(2)	2.677(2)	2.675(3)	2.672(2)
Yb(2)–S(4) × 2	2.613(1)	2.621(2)	2.619(2)

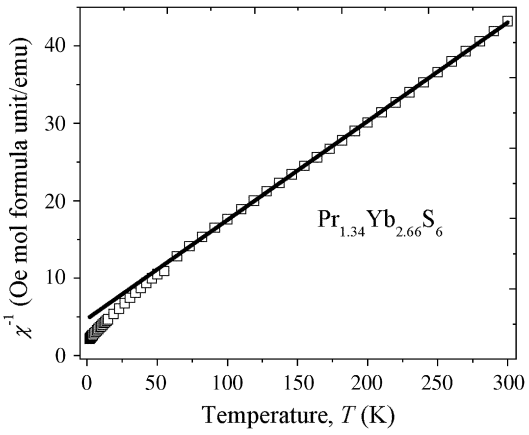

Fig. 3. Inverse molar magnetic susceptibility plotted against temperature between 2 and 300 K for $Pr_{1.34}Yb_{2.66}S_6$. Data were taken under an applied magnetic field of 0.1 T. The straight line represents the fit to Curie–Weiss law in the range of 100–300 K.

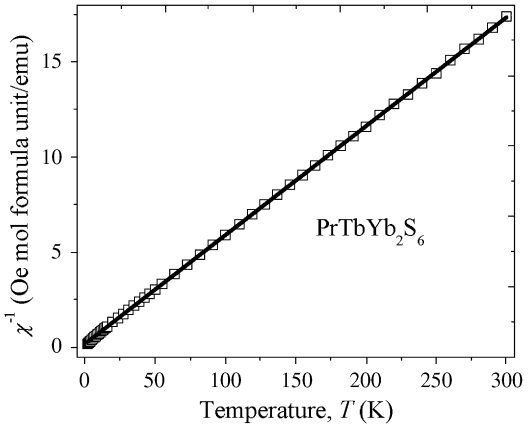

Fig. 4. The plot of the inverse molar magnetic susceptibility vs T for $PrTbYb_2S_6$ under an applied magnetic field of 0.1 T between 2 and 300 K. The straight line represents the fit to Curie–Weiss law in the range of 100–300 K.

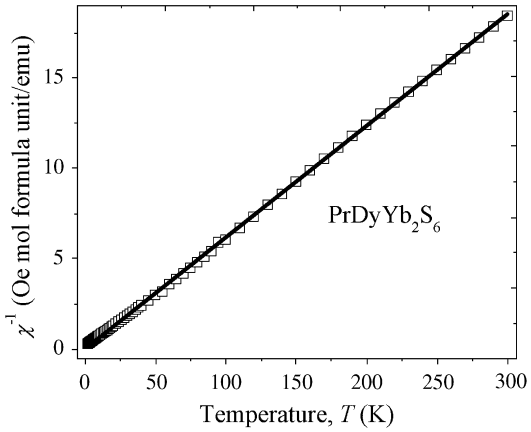

Fig. 5. The temperature dependence of the reciprocal molar magnetic susceptibility for $PrDyYb_2S_6$ under an applied magnetic field of 0.1 T between 2 and 300 K. The straight line represents the fit to Curie–Weiss law in the range of 100–300 K.

Table 6
Magnetic parameters for Pr*Ln*Yb_2S_6 (*Ln* = Pr/Yb, Tb, Dy)

Formula	P_{cal}/μ_B[a]	P_{eff}/μ_B[a]	θ_p/K[b]	R^{2b}
$Pr_{1.34}Yb_{2.66}S_6$	8.48	7.91(1)	−36.9(8)	0.99979
$PrTbYb_2S_6$	12.19	11.82(1)	−3.1(4)	0.99992
$PrDyYb_2S_6$	12.92	11.38(2)	−0.2(7)	0.99979

[a] P_{cal} and P_{eff}: calculated [30] and experimental effective magnetic moments per formula unit.
[b] Weiss constant (θ_p) and goodness of fit (R^2) obtained from high-temperature (100–300 K) data.

effective magnetic moments for these compounds are close to the calculated values [30]. This provides further supporting evidence for the proposed formula from the single-crystal X-ray experiments.

3.3. Optical properties

The UV–vis–NIR diffuse reflectance spectra of Pr*Ln*Yb_2S_6 (*Ln* = Pr/Yb, Tb, Dy) are presented in Fig. 6. They are very similar to one another. This suggests that the substitutions using different lanthanides ions in the seven-coordinate *Ln* positions make small changes of the band structures near the Fermi level for Pr*Ln*Yb_2S_6 (*Ln* = Pr/Yb, Tb, Dy). The optical transition is constituted primarily from the interactions among eight-coordinate Pr^{3+} cations, six-coordinate Yb^{3+} cations, and S^{2-} anions. It is also possible that the 4*f*-band of Pr, Yb, Tb, and Dy lie deep in the valence band. Therefore the optical transitions are determined by the same gap between the [S]3*p* valence band and 5*d*(6*s*) conduction band [31,32]. The band gaps of Pr*Ln*Yb_2S_6 (*Ln* = Pr/Yb, Tb, Dy) are approximately 1.6 eV, which are consistent with the dark red color they possess. They are also close to the values reported for γ-*LnLn*′S_3 (*Ln* = La, Ce; *Ln*′ = Er, Tm, Yb) [13] and δ-$Ln_{2-x}Lu_xS_3$ (*Ln* = Ce, Pr, Nd; $x = 0.67-0.71$) [14].

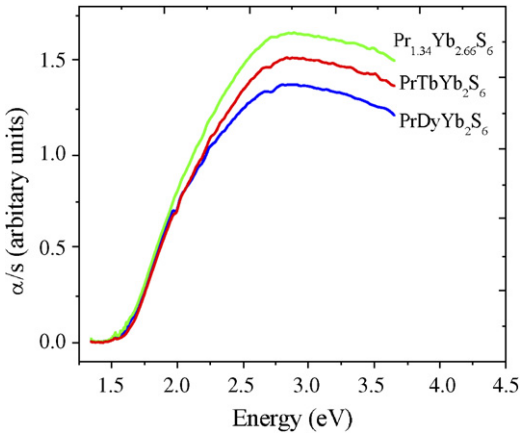

Fig. 6. UV–vis diffuse reflectance spectra of Pr*Ln*Yb_2S_6 (*Ln* = Pr/Yb, Tb, Dy).

4. Conclusions

The first two partially ordered quaternary interlanthanide sulfides Pr*Ln*Yb_2S_6 (*Ln* = Tb, Dy) were prepared and characterized. They adopt the same F-Ln_2S_3-type structure as the parent disordered $Pr_{1.34}Yb_{2.66}S_6$ phase. All three compounds are paramagnetic in the range of 2 and 300 K. The UV–vis–NIR diffuse reflectance spectra show that these compounds have very similar electronic structures near the Fermi level with wide band gaps. The elemental analysis and magnetic susceptibility measurements are consistent with the proposed formula.

Acknowledgments

This work was supported by the US Department of Energy under Grant DE-FG02-02ER45963 through the EPSCoR Program. Funds for purchasing the UV–vis–NIR spectrometer used in these studies were provided through the Chemical Sciences, Geosciences and Biosciences Division, Office of Basic Energy Sciences, Office of Science, Heavy Elements Program, US Department of Energy under Grant DE-FG02-01ER15187. JSB and ESC acknowledge support from NSF-DMR 0203532. A portion of this work was performed at the National High Magnetic Field Laboratory, which is supported by the National Science Foundation Cooperative Agreement No. DMR-0084173, by the State of Florida, and by the Department of Energy.

References

[1] N. Rodier, P. Laruelle, C.R. Seances, Acad. Sci. Ser. C 270 (1970) 2127.
[2] D.J.W. Ijdo, Acta Crystallogr. B 36 (1980) 2403.
[3] N. Rodier, R. Julien, V. Tien, Acta Crystallogr. C 39 (1983) 670.
[4] K.-J. Range, A. Gietl, U. Klement, Z. Kristallogr. 207 (1993) 147.
[5] N. Rodier, R.L. Firor, V. Tien, M. Guittard, Mater. Res. Bull. 11 (1976) 1209.
[6] N. Rodier, V. Tien, C. R. Acad. Sci. Paris Ser. C 279 (1974) 817.
[7] N. Rodier, P. Laruelle, Bull. Soc. Fr. Mineral Cristallogr. 95 (1972) 548.
[8] F. Hulliger, O. Vogt, Phys. Lett. 21 (1966) 138.
[9] W. Lugscheider, H. Pink, K. Weber, W. Zinn, Z. Angew. Phys. 30 (1970) 36.
[10] P. Lemoine, D. Carre, M. Guittard, Acta Crystallogr. C 41 (1985) 667.
[11] D. Carré, P. Laruelle, Acta Crystallogr. B 30 (1974) 952.
[12] K. Mitchell, R.C. Somers, F.Q. Huang, J.A. Ibers, J. Solid State Chem. 177 (2004) 709.
[13] G.B. Jin, E.S. Choi, R.P. Guertin, J.S. Brooks, T.H. Bray, C.H. Booth, T.E. Albrecht-Schmitt, Chem. Mater. 19 (2007) 567.
[14] G.B. Jin, E.S. Choi, R.P. Guertin, J.S. Brooks, T.H. Bray, C.H. Booth, T.E. Albrecht-Schmitt, J. Solid State Chem. 180 (2007) 2129.
[15] N. Rodier, Bull. Soc. Fr. Mineral. Cristallogr. 96 (1973) 350.
[16] D.L. Gray, B.A. Rodriguez, G.H. Chan, R.P. Van Duyne, J.A. Ibers, J. Solid State Chem. 180 (2007) 1527.
[17] D. Carré, P. Laruelle, Acta Crystallogr. B 29 (1973) 70.
[18] N. Rodier, V. Tien, Bull. Soc. Fr. Mineral. Cristallogr. 98 (1975) 30.
[19] M. Marezio, J.P. Remeika, P.D. Dernier, Acta Crystallogr. B 26 (1970) 2008.
[20] T. Schleid, F. Lissner, J. Alloys Compd. 189 (1992) 69.
[21] C.M. Fang, A. Meetsma, G.A. Wiegers, J. Alloys Compd. 201 (1993) 255.
[22] C. Adolphe, Ann. Chimie (Paris) 10 (1965) 271.
[23] D.F. Becker, J.S. Kasper, Acta Crystallogr. 10 (1957) 332.
[24] H. Noël, J. Padiou, Acta Crystallogr. B 32 (1976) 1593.
[25] G.M. Sheldrick, SHELXTL PC, Version 6.12, An Integrated System for Solving, Refining, and Displaying Crystal Structures from Diffraction Data; Siemens Analytical X-ray Instruments, Inc., Madison, WI, 2001.
[26] G.M. Sheldrick, *SADABS* 2001, Program for absorption correction using SMART CCD based on the method of Blessing: Blessing R.H., Acta Crystallogr. A 51 (1995) 33.
[27] R.D. Shannon, Acta Crystallogr. A 32 (1976) 751.
[28] L.N. Mulay, E.A. Boudreaux, Theory and Applications of Molecular Diamagnetism, Wiley–Interscience, New York, 1976.
[29] W.W. Wendlandt, H.G. Hecht, Reflectance Spectroscopy, Interscience Publishers, New York, 1966.
[30] C. Kittel, Introduction to Solid State Physics, 6th ed., Wiley, New York, 1986.
[31] A.V. Prokofiev, A.I. Shelykh, A.V. Golubkov, I.A. Smirnov, J. Alloys Compd. 219 (1995) 172.
[32] A.V. Prokofiev, A.I. Shelykh, B.T. Melekh, J. Alloys Compd. 242 (1996) 41.